Tunable topological Weyl semimetal from simple-cubic lattices with staggered fluxes

Jian-Hua Jiang*

Department of Condensed Matter Physics, Weizmann Institute of Science, Rehovot 76100, Israel

(Received 2 January 2012; published 28 March 2012)

Three-dimensional Weyl fermions are found to emerge from simple-cubic lattices with staggered fluxes. The mechanism is a gapping of the quadratic-band touching by time-reversal-symmetry-breaking hoppings. The system exhibits a rich phase diagram where the number of Weyl fermions and their topological charges are tunable via plaquette fluxes. The Weyl semimetal state is shown to be the intermediate phase between a nontopological semimetal and a quantum anomalous Hall insulator. The transitions between those phases can be understood through the evolution of the Weyl points as Berry-flux insertion processes. As the Weyl points move and split (or merge) through tuning of the plaquette fluxes, the Fermi arcs and surface states undergo significant manipulation. We also propose a possible scheme to realize the model in ultracold fermions in optical lattices with artificial gauge fields.

DOI: 10.1103/PhysRevA.85.033640 PACS number(s): 03.75.Ss, 71.10.Fd, 05.30.Fk, 03.65.Vf

I. INTRODUCTION

Massless Dirac fermions possess chiral symmetry and can be classified by their chirality γ. For example, in three dimensions (3D), if the Hamiltonian is $H = v_F \boldsymbol{\sigma} \cdot \mathbf{q}$ where $|v_F|$ is the Fermi velocity, $\boldsymbol{\sigma}$ is the vector of Pauli matrices, and $\mathbf{q}$ is the wave vector, then the chirality is $\gamma = \mathrm{sgn}(v_F)$. Such fermions (also called chiral or Weyl fermions) possess several peculiar behaviors such as the Adler-Bell-Jackiw anomaly [1]. Chiral fermions in two dimensions (2D) have been found in real condensed-matter systems since the discovery of graphene [2]. Many novel electronic properties of graphene [3]—Klein tunneling, the peculiar integer quantum Hall effect, transport properties such as the conductivity minimum, the weak (anti)localization, and edge states—originate from its chiral fermion nature. Recent studies also found realizations of 2D chiral fermions in ultracold-atomic-gas optical lattices [4]. A generic route to chiral fermions is to search systems in which two bands touch [5]. Around the band-touching node, the Hamiltonian can generally be written as $H = \mathbf{h}(\mathbf{k}) \cdot \boldsymbol{\sigma}$, where the Pauli matrices $\boldsymbol{\sigma}$ act on the space spanned by the two bands and $|\mathbf{h}| \to 0$ at the node. For example, in graphene, around one of the nodes $\mathbf{K}$, $\mathbf{h}(\mathbf{k} + \mathbf{K}) = v_F \mathbf{k}$. Thus chiral fermions emerge as topological defects (vortices) in $\mathbf{k}$ space. They are generally classified by their vortex winding number N_w. In the special cases when $N_w = \pm 1$, the winding number gives the chirality, $\gamma = N_w$. In general cases, N_w can be any integer. The total winding number in the system must be conserved under adiabatic transformation. The winding number can be defined by the Berry phase carried by the node, $N_w = \frac{1}{\pi} \oint_\Gamma d\mathbf{k} \cdot \langle \Psi(\mathbf{k}) | i \nabla_{\mathbf{k}} | \Psi(\mathbf{k}) \rangle$, where Γ is a contour enclosing the node and $\Psi(\mathbf{k})$ is the single-valued and continuous wave function of the eigenstates with $H|\Psi(\mathbf{k})\rangle = \pm|\mathbf{h}(\mathbf{k})||\Psi(\mathbf{k})\rangle$. By breaking the time-reversal symmetry, such two-band touching can be gapped, leading to a quantum anomalous Hall (QAH) insulator with Chern number $C = \pm\frac{1}{2} N_w$ [6].

3D Weyl fermions are more robust: they cannot be gapped even by time-reversal-symmetry breaking. In fact they can only be annihilated in pairs with the total winding number conserved under adiabatic transformations. The winding number of 3D Weyl fermions is defined as [7] $N_w = \frac{1}{8\pi} \varepsilon^{\nu\delta\rho} \oint_{\mathcal{S}} dS^\rho \hat{\mathbf{n}} \cdot (\partial_{k_\nu} \hat{\mathbf{n}} \times \partial_{k_\delta} \hat{\mathbf{n}})$ ($\nu, \delta, \rho = x, y, z$ and ε is the Levi-Cività tensor), where $\mathcal{S}$ is a surface enclosing the band-touching node (Weyl point), dS^ρ represents the surface area elements along the ρ direction, and $\hat{\mathbf{n}} = \mathbf{h}/|\mathbf{h}|$. 3D Weyl fermions are monopoles of the Berry-phase gauge fields where the monopole charge is the topological charge N_w [7]. As a consequence, there is a step change in the Hall conductivity, e.g., $\sigma_{xy}(k_z)$ [and the Chern number $C_{xy}(k_z) = \frac{h}{e^2} \sigma_{xy}(k_z)$], as a function of k_z,

$$\sigma_{xy}(k_z) = \mathrm{sgn}\left(k_z - k_z^c\right) \frac{N_w}{2} \frac{e^2}{h} + \cdots, \tag{1}$$

due to the monopole at k_z^c; the ellipsis denotes other contributions to the Hall conductivity (Chern number). According to the Nielsen-Ninomiya theorem [8], Weyl points must appear in pairs with opposite N_w in a lattice system.

The Weyl semimetal (a system with 3D Weyl fermions) possesses very special properties such as chiral surface states with open Fermi surfaces (Fermi arcs) terminating at the projection of the Weyl points, and thickness-dependent quantized anomalous Hall conductivity in thin films, which were first found in studies of ^{3}He-A [7,9]. After that Murakami showed that a Weyl semimetal phase can appear as an intermediate phase between a normal insulator and a topological insulator [10]. Recent studies demonstrate that Weyl semimetals can also be realized in other condensed-matter systems [11]: some pyrochlore iridates (such as $Y_2Ir_2O_7$) [12], superlattices made of topological insulator and nontopological insulator thin films with broken time-reversal [13,14] or inversion [15] symmetry, the ferromagnetic compound $HgCr_2Se_4$ [16,17], and bulk magnetically doped Bi_2Se_3 [18]. It is also found that in some situations the number and type of the Weyl points are determined and protected by the lattice symmetries [17,19]. Topological nodal semimetals where the bulk spectrum exhibits nodal lines were also proposed and studied in Ref. [14]. There are also some lattice models where Weyl fermions are found [20].

In this work we show that Weyl fermions can emerge from simple-cubic lattices with staggered fluxes through plaquettes (see Fig. 1). Unlike previous studies where the Weyl

*jianhua.jiang.phys@gmail.com

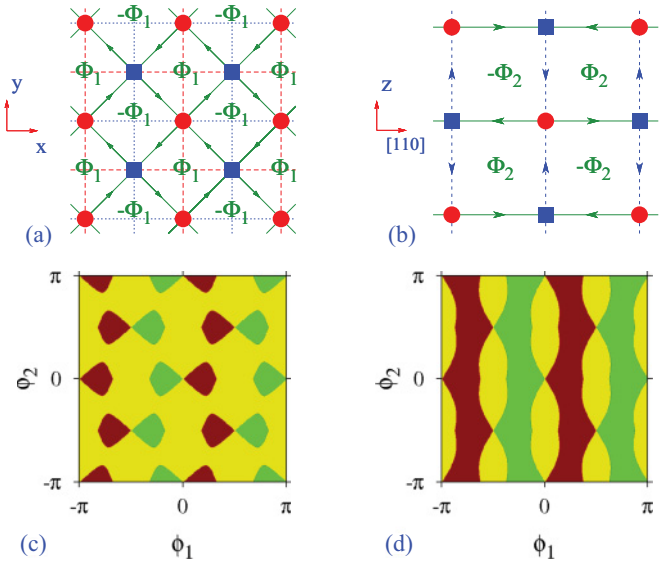

FIG. 1. (Color online) Lattice structure in (a) (001) plane in an odd layer and (b) $(1\bar{1}0)$ plane. Red dots and blue squares represent type-A and -B sites, respectively. Hoppings along (opposite) the green solid and blue dotted arrows are $t_2 e^{-i\phi_1}$ and $t_\perp e^{-i\phi_2}$ ($t_2 e^{i\phi_1}$ and $t_\perp e^{i\phi_2}$) separately. Those along the red dashed and blue dotted lines are t_y and t_x, respectively. $\pm\Phi_1$ and $\pm\Phi_2$ are the plaquette fluxes. In the phase diagram (c) $|t_2/t_\perp| = 0.95$ and in (d) $|t_2/t_\perp| = 1.3$. Yellow region, Weyl semimetal; green region, QAH state with Chern number $C_{xy}(k_z) = -2\mathrm{sgn}(t_1 t_2 t_\perp)$ for all k_z; brown region, QAH state with $C_{xy}(k_z) = 2\mathrm{sgn}(t_1 t_2 t_\perp)$ for all k_z.

semimetal phases emerge due to inverted bands with spin-orbit interactions [10,15–17] or gaping Dirac cones from various mass terms [13,14,18], here the mechanism is to gap the quadratic-band touching via time-reversal-symmetry-breaking hoppings due to the staggered fluxes. A direct distinction is that this scenario does not need to invoke spin-degeneracy breaking (i.e., spin-orbit coupling). The system exhibits rich phase diagrams where the number of Weyl fermions and their topological charge are tunable via the fluxes per plaquettes. The Weyl semimetal state is demonstrated as the intermediate phase between a nontopological semimetal and a quantum anomalous Hall insulator. The transitions between those phases can be understood via the evolution of the Weyl points as Berry-flux insertion processes (see Sec. IV and the Summary). As the Weyl points move and split (or merge) through tuning of the plaquette fluxes, the Fermi arcs and surface states undergo significant change, because the Fermi arcs act as Dirac strings which have to connect the monopoles with opposite charges. Finally, we propose a possible scheme to realize this model in ultracold fermionic gases in optical lattices with artificial gauge fields.

II. LATTICE AND HAMILTONIAN

We consider a simple-cubic lattice system, which can be viewed as stacking of layers of 2D lattices with checkerboard-patterned staggered fluxes (see Fig. 1) [21–24]. The 2D checkerboard lattice is designed in such a way that the hoppings between the nearest-neighbor A-type sites along the x and y directions are t_x and t_y, respectively, whereas those for B-type sites are t_y and t_x, respectively [see Fig. 1(a)]. The hoppings from the A-type to the nearest B-type sites are $t_2 e^{\pm i\phi_1}$, as indicated in Fig. 1(a). The flux per plaquette is $\pm\Phi_1 = \pm 4\phi_1$ [Fig. 1(a)]. Recently Sun *et al.* proposed a realistic optical lattice system to realize such a model [21]. Additionally, it can be realized in ultracold fermions in optical lattices and in condensed-matter systems with artificial [25–29] or "emergent" [30] gauge fields. The Hamiltonian for each layer is [21–24] $H_{2D} = h_0(\mathbf{k})\sigma_0 + \mathbf{h}_1(\mathbf{k})\cdot\boldsymbol{\sigma}$, where $\boldsymbol{\sigma}$ is the Pauli matrix vector acting on the (B) [pseudospin up (down)] site space and σ_0 is the 2×2 identity matrix. As there is no need to invoke true-spin splitting, we keep the true-spin states as degenerate. $h_0(\mathbf{k}) = 2t_0(\cos k_x + \cos k_y)$, $h_{1z}(\mathbf{k}) = 2t_1(\cos k_x - \cos k_y)$, $h_{1x}(\mathbf{k}) = 4t_2 \cos\phi_1 \cos\frac{k_x}{2}\cos\frac{k_y}{2}$, and $h_{1y}(\mathbf{k}) = 4t_2 \sin\phi_1 \sin\frac{k_x}{2}\sin\frac{k_y}{2}$, where $t_0 = (t_x + t_y)/2$ and $t_1 = (t_x - t_y)/2$. (Note that throughout this paper, we set the lattice constant $a = 1$. All the wave vectors are then in units of $1/a = 1$.) The two bands touch quadratically at (π,π) when $\sin\phi_1 = 0$. This band touching is nontrivial as it carries a nonzero winding number $N_w = 2\mathrm{sgn}(t_1 t_2 \cos\phi_1) = \pm 2$. At finite $\sin\phi_1$ (broken time-reversal symmetry), the quadratic-band touching is gapped and the system becomes a QAH insulator with Chern number $C = \frac{1}{2}\mathrm{sgn}(t_2 \sin\phi_1) N_w$ [22,23].

The 3D lattice is a stacking of the 2D layers in such a way that different types of site are on top of each other [see Fig. 1(b)]. The hopping between those sites is $t_\perp e^{\pm i\phi_2}$. The staggered flux per plaquette in the $(1\bar{1}0)$ plane is $\pm\Phi_2 = \pm 2(\phi_1 + \phi_2)$ [in the (110) plane, the plaquette flux is $\pm 2(\phi_1 - \phi_2)$]. The Hamiltonian of the system is then

$$H = [h_0(\mathbf{k})\sigma_0 + \mathbf{h}(\mathbf{k})\cdot\boldsymbol{\sigma}]\tau_0 + g(k_z)(\cos\phi_2\sigma_x + \sin\phi_2\sigma_y)\tau_x. \tag{2}$$

Here the σ and τ matrices act on the A (B) sites and odd (even) layers, respectively. $g(k_z) = 2t_\perp \cos\frac{k_z}{2}$. The Hamiltonian can be block diagonalized directly, giving

$$H_\pm = h_0(\mathbf{k})\sigma_0 + \mathbf{h}_\pm(\mathbf{k})\cdot\boldsymbol{\sigma} \tag{3}$$

in the two blocks, where

$$\begin{aligned} h_{\pm x}(\mathbf{k}) &= 4t_2 \cos\phi_1 \cos\frac{k_x}{2}\cos\frac{k_y}{2} \pm g(k_z)\cos\phi_2, \\ h_{\pm y}(\mathbf{k}) &= 4t_2 \sin\phi_1 \sin\frac{k_x}{2}\sin\frac{k_y}{2} \pm g(k_z)\sin\phi_2, \\ h_{\pm z}(\mathbf{k}) &= 2t_1(\cos k_x - \cos k_y). \end{aligned} \tag{4}$$

For the sake of easier formulation, we set the first Brillouin zone as $k_x \in [0,2\pi]$, $k_y \in [0,2\pi]$, and $k_z \in [0,2\pi]$. Finally, the system possesses a series of inversion symmetries. It is invariant under the following inversion transformations: (i) $z \to -z$, (ii) $(x,y) \to (-x,-y)$, and (iii) $(x,y,z) \to (-x,-y,-z)$. At $h_0 = 0$, the system also has particle-hole symmetry.

III. PHASE DIAGRAMS

The energy spectrum of the system is

$$E_{\alpha\pm}(\mathbf{k}) = h_0(\mathbf{k}) \pm |\mathbf{h}_\alpha(\mathbf{k})| \tag{5}$$

with $\alpha = \pm$. The equations for the nodes (Weyl points) are $h_{\alpha x} = h_{\alpha y} = h_{\alpha z} = 0$. One finds that away from ϕ_1 or

$\phi_2 = 0, \pm\pi/2, \pi$ (see Fig. 1 and discussion below), there are four Weyl points $\mathbf{K}_{+\beta} = (\beta k_x^c, \beta k_y^c, k_z^c)$ ($\beta = \pm$) in the + block and $\mathbf{K}_{-\beta} = (\beta k_x^c, \beta k_y^c, 2\pi - k_z^c)$ in the − block, where

$$k_y^c = \pi - 2\arctan\sqrt{\left|\frac{\tan\phi_1}{\tan\phi_2}\right|},$$
$$k_x^c = \eta k_y^c \quad \text{with} \quad \eta = \mathrm{sgn}\left(\frac{\tan\phi_1}{\tan\phi_2}\right), \tag{6}$$
$$k_z^c = 2\arccos\left[\frac{-2\eta t_2 \sin\phi_1}{t_\perp \sin\phi_2}\left(1 + \left|\frac{\tan\phi_1}{\tan\phi_2}\right|\right)^{-1}\right].$$

Note that the above equation holds only when

$$\left|\frac{2t_2 \sin\phi_1}{t_\perp \sin\phi_2}\left(1 + \left|\frac{\tan\phi_1}{\tan\phi_2}\right|\right)^{-1}\right| \leqslant 1, \tag{7}$$

which sets the phase boundaries of the Weyl semimetal. It is required that $|h_0(\mathbf{k}) - h_0(\mathbf{K}_{\alpha\beta})| \leqslant |\mathbf{h}_\alpha(\mathbf{k})|$ so that the system is an insulator everywhere away from the nodes $\mathbf{K}_{\alpha\beta}$ (the definition of a semimetal). Given this, the $h_0(\mathbf{k})\sigma_0$ term is irrelevant for the physics to be discussed, and we hence take $h_0 \equiv 0$ hereafter.

In Figs. 1(c) and 1(d) we plot the phase diagram at two different $|t_2/t_\perp|$. There are three phases: the Weyl semimetal, the QAH insulator, and the nontopological semimetal. The last one refers to semimetals that have only nodes with $N_w = 0$. Such nodes are accidental band-degeneracy points, which can be gapped by infinitesimal band mixing without breaking any symmetries. The QAH phase actually consists of two topologically distinct phases with opposite Chern numbers [$C_{xy}(k_z) = \pm 2\mathrm{sgn}(t_1 t_2 t_\perp)$ for all k_z]. Those two phases are separated by the Weyl semimetal and nontopological semimetal phases. In fact, the Weyl semimetals can be viewed as intermediate phases between the nontopological semimetal (or insulator) phase and the QAH phase. In the former the Chern number is always zero, whereas in the latter it is always nonzero. In Weyl semimetals, there are two regions in the Brillouin zone: the Chern number is zero in one region and nonzero in the other. Specifically, in the current model $C_{xy}(k_z)$ is nonzero only when $k_z \in (k_z^{\min}, k_z^{\max})$ with $k_z^{\min} = \mathrm{Min}(k_z^c, 2\pi - k_z^c)$ and $k_z^{\max} = \mathrm{Max}(k_z^c, 2\pi - k_z^c)$. The QAH and nontopological semimetal phases can be viewed as the limits $k_z^{\min} \to 0$ and $k_z^{\min} \to \pi$, respectively. There are actually two Weyl semimetal phases with Chern numbers $C_{xy}(k_z)$ of opposite signs at $k_z \in (k_z^{\min}, k_z^{\max})$. Those two states are the intermediate states between the two QAH states (with opposite Chern numbers) and the nontopological semimetal state separately. The latter lies at the lines $\phi_1 = 0, \pm\pi/2$, and π in the phase diagrams, where $k_z^{\min} = k_z^{\max} = \pi$. We will show in the next section that the evolution of the ground state and quantum phase transitions between those phases can be understood via the evolution of the Weyl points as Berry-flux insertion processes.

We find that, as $|t_2/t_\perp|$ increases, the area of the Weyl semimetal phase in the phase diagram as a function of ϕ_1 and ϕ_2 shrinks. At $|t_2/t_\perp| \to \infty$, this area becomes zero. When $|t_2/t_\perp| \leqslant 1/2$ the system is always in the Weyl semimetal phase except at the special lines $\phi_1 = 0, \pm\pi/2, \pi$. Hence the region of the Weyl semimetal phases *can be tuned by the ratio* $|t_2/t_\perp|$. It is noted that the phase diagram exhibits some angle-shaped structures around the special points $(\phi_1, \phi_2) = (\phi_c, \pm\phi_c)$, with $\phi_c = 0, \pm\pi/2, \pi$, as well as $(0,\pi)$ and $(\pi,0)$ where Eq. (6) becomes ill defined. The structure around, say, (0,0), can be understood via the following analysis. For (ϕ_1, ϕ_2) close to (0,0), along the line $\phi_2 = \xi\phi_1$, $k_z^c = 2\arccos[-2t_2/t_\perp(|\xi| + 1)]$. Hence the Weyl semimetal phase is at $|\xi| > |2t_2/t_\perp| - 1$, which is angular. When $|t_2/t_\perp| < 1/2$, the system is in the Weyl semimetal phase for all parameters (ϕ_1, ϕ_2) around (0,0).

It is worthwhile to point out some special regions in the phase diagram. First, when $\phi_2 = \pm\pi/2$, there are only two Weyl points: $\mathbf{K}_+ = (\pi, \pi, k_z^c)$ in the + block and $\mathbf{K}_- = (\pi, \pi, 2\pi - k_z^c)$ in the − block. Those Weyl points are quadratic-band touchings with winding number $N_w = \pm 2$. Similarly, when $\phi_2 = 0, \pi$, there are two quadratic-band-touching Weyl points: $\mathbf{K}_+ = (0, 0, k_z^c)$ in the + block and $\mathbf{K}_- = (0, 0, 2\pi - k_z^c)$ in the − block. In addition, as pointed out before, at the lines $\phi_1 = 0, \pm\pi/2, \pi$ the system is a nontopological semimetal.

IV. EVOLUTION OF WEYL POINTS

Away from the above regions, there are four Weyl points, around which fermions are described by the Weyl Hamiltonian

$$H_{\alpha\beta}(\mathbf{k}) = \boldsymbol{\sigma} \cdot \hat{v}_{\alpha\beta} \cdot \mathbf{q} + O(q^2), \tag{8}$$

where $\mathbf{q} = \mathbf{k} - \mathbf{K}_{\alpha\beta}$. The velocity tensors of the Dirac cones are

$$\hat{v}_{\alpha\beta} = \begin{pmatrix} -\beta\eta t_2 \cos\phi_1 \sin k_y^c & -\beta t_2 \cos\phi_1 \sin k_y^c & -\alpha t_\perp \cos\phi_2 \sin\frac{k_z^c}{2} \\ \beta t_2 \sin\phi_1 \sin k_y^c & \beta\eta t_2 \sin\phi_1 \sin k_y^c & -\alpha t_\perp \sin\phi_2 \sin\frac{k_z^c}{2} \\ -2\beta\eta t_1 \sin k_y^c & 2\beta t_1 \sin k_y^c & 0 \end{pmatrix}. \tag{9}$$

The winding number is the sign of the determinator of the velocity tensor, $N_w(\alpha\beta) = \mathrm{sgn}[\det(\hat{v}_{\alpha\beta})]$. One finds

$$N_w(\alpha\beta) = -\alpha\,\mathrm{sgn}[t_1 t_2 t_\perp \sin(\phi_1 + \eta\phi_2)]. \tag{10}$$

Note that Weyl points in the same block α have the same topological charge (independent of β), whereas Weyl points in different blocks have opposite topological charges. The positions and motions of the four Weyl points are illustrated in Fig. 2 for a specific case where $N_w = -\alpha$, $k_y^c = -k_x^c < \pi$, and $k_z^c > \pi$. According to Eq. (1), the Chern number $C_{xy}(k_z)$ varies with k_z. The Chern number changes only when the gap is closed and reopened, i.e., when k_z passes through k_z^c and

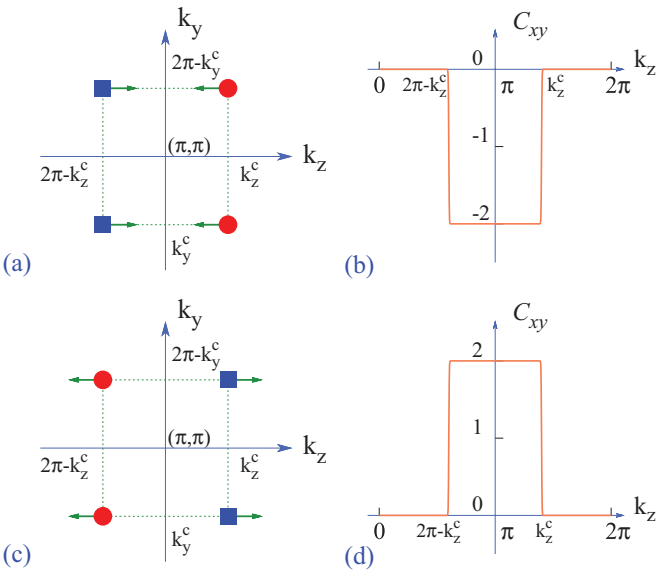

FIG. 2. (Color online) (a),(c) Illustration of the Weyl points when there are four in the k_y-k_z plane. The arrows indicate the z-direction movement of the Weyl points as ϕ_1 increases. Blue squares (red dots) denote Weyl points with $N_w = -1$ ($N_w = 1$). The parameters are $t_1 = 1$, $t_2 = 2$, $t_\perp = 2$, and $\phi_2 = -0.25\pi$. $\phi_1 = -0.1\pi$ in (a), and $\phi_1 = 0.1\pi$ in (c). (b),(d) Chern number $C_{xy}(k_z)$ as a function of k_z for the cases in (a) and (c), respectively.

$2\pi - k_z^c$. The Chern number is calculated as

$$C_{xy} = \sum_{\alpha=\pm} \frac{1}{4\pi} \int_0^{2\pi} dk_x \int_0^{2\pi} dk_y \mathbf{n}_\alpha \cdot \left(\partial_{k_x} \mathbf{n}_\alpha \times \partial_{k_y} \mathbf{n}_\alpha\right), \quad (11)$$

where $\mathbf{n}_\alpha = \mathbf{h}_\alpha/|\mathbf{h}_\alpha|$. We find that $C_{xy}(k_z) = 2\mathrm{sgn}[t_1 t_2 t_\perp \sin(2\phi_1)]$ when $k_z \in (k_z^{\min}, k_z^{\max})$, otherwise $C_{xy}(k_z) = 0$. The relation between the quantum phase transitions and the evolution of the Weyl points is depicted in Fig. 2 where we consider a situation with $\phi_2 = -0.25\pi$ and ϕ_1 varying from -0.1π to 0.1π. At $\phi_1 = -0.1\pi$, the Weyl points with $N_w < 0$ are in the $k_z < \pi$ region whereas those with $N_w > 0$ are in the $k_z > \pi$ region [Fig. 2(a)]. Consequently, the Chern number $C_{xy}(k_z)$ is negative at $k_z \in (k_z^{\min}, k_z^{\max})$. As ϕ_1 increases the Weyl points with $N_w < 0$ and those with $N_w > 0$ move in opposite directions along k_z and become closer together. At $\phi_1 = 0$, Weyl points with opposite N_w *coincide* and the system becomes a nontopological semimetal. After that their positions *shift* as ϕ_1 increases [Fig. 2(c)]: the Weyl points with $N_w < 0$ move into the $k_z > \pi$ region whereas those with $N_w > 0$ move to the $k_z < \pi$. As a consequence the Chern number $C_{xy}(k_z)$ changes sign at $k_z \in (k_z^{\min}, k_z^{\max})$. Further variation of ϕ_1 will enlarge the region and finally the system becomes a QAH insulator after $k_z^{\min} \to 0$ where pairs of monopoles with opposite topological charge (N_w) merge and annihilate each other. During those processes *quantized Berry fluxes are inserted into each k_x-k_y plane with fixed k_z, whenever the monopoles move across it*, as there are quantized Berry fluxes flowing between monopoles with opposite charges.

In addition, as $\phi_2 \to 0$, $\pm\pi/2$, and π, the two Dirac cones with the same k_z merge together and form a quadratic-band touching as they have the same winding number. The k_z dependence of $C_{xy}(k_z)$ in this situation is similar to the previous one. However, as we will show later, the Fermi arcs and surface states in those two situations are significantly different.

V. EVOLUTION OF FERMI ARCS AND SURFACE STATES

The movement and merging (or splitting) of the Weyl points have profound effects on the topologically protected surface states. In particular, we demonstrate the Fermi arcs on the surface for two situations where there are (i) four Dirac cones and (ii) two quadratic-band touchings in Figs. 3(a) and 3(b), respectively. The color represents the spectral function $\mathcal{A}(E) = \frac{-1}{\pi}\mathrm{Im}G^r(E)$ [$G^r(E)$ is the retarded Green function of the system] of the zero-energy ($E = 0$) surface states (i.e., the Fermi arcs). The surface is perpendicular to the x direction. It is noted that although the k_z dependence of $C_{xy}(k_z)$ is similar in the two cases, the Fermi arcs are quite different. This is essentially due to the different positions of the monopoles in $\mathbf{k}$ space. From Fig. 3(c), one can see that *the zero-energy surface states (Fermi arcs) merge into the bulk bands through the Weyl points*. This figure clearly visualizes the fact that Fermi arcs are Dirac strings which link the monopoles and antimonopoles of opposite "magnetic"

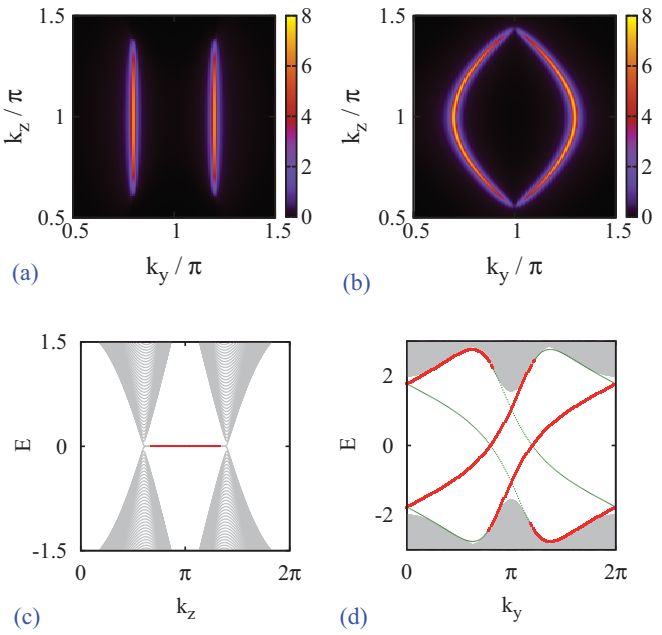

FIG. 3. (Color online) Spectral function $\mathcal{A}(E)$ of the surface states at zero energy ($E = 0$) in the case with (a) four Dirac cones and (b) two quadratic-band touchings. Spectra of surface and bulk states as functions of (c) k_z (at $k_y = 0.8\pi$) and (d) k_y (at $k_z = \pi$) with the same parameters as in (a). The size of the system is 151 unit cells (due to the finite-size effect the bulk bands are slight gapped at the node). The gray region represents bulk spectra, while red thick (green thin) curves denote the surface spectra at the left (right) boundary. [Note that in (c) the surface spectra at the two boundaries coincide.] $t_1 = 1$, $t_2 = 2$, and $t_\perp = 2$. In (a), (c), and (d) $\phi_1 = 0.1\pi$, $\phi_2 = -0.25\pi$, whereas in (b) $\phi_1 = 0.15\pi$, $\phi_2 = -0.5\pi$. Correspondingly, $k_y^c = 0.8\pi$ and $k_z^c = 1.4\pi$ in (a), (c), and (d), whereas $k_y^c = \pi$ and $k_z^c = 1.5\pi$ in (b). The results are calculated via the iterative Green function method in Ref. [31]. An artificial spectral broadening 0.04 is used for the sake of visibility.

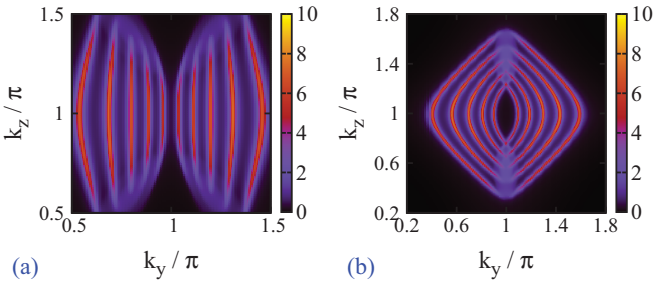

FIG. 4. (Color online) Spectral functions of the surface states for two cases: (a) four Dirac cones; (b) two quadratic-band touchings. The energies of the surface states from left to right (in both the $k_y < \pi$ and $k_y > \pi$ regions) are -0.8, -0.4, 0, 0.4, and 0.8, respectively. For example, both the leftmost arc in the $k_y < \pi$ region and the leftmost arc in the $k_y > \pi$ region have energy -0.8. The parameters for (a) and (b) are the same as those in Figs. 3(a) and 3(b), respectively. An artificial spectral broadening 0.04 is used for the sake of visibility.

charges (N_w) in the Berry-phase gauge fields [7]. As Fermi arcs terminate at the Weyl points, the positions of the monopoles are essential to the shape of the Fermi arcs and the topologically protected surface state spectra. From the figure it is seen that the monopole-antimonopole pair with the same k_y (but opposite k_z) is connected via the Dirac strings. This string configuration is due to the facts that (i) the system possesses inversion symmetry $k_z \to -k_z$; (ii) the string connecting the monopoles and antimonopoles must pass through the $k_z = \pi$ plane because it exists only in the region $k_z \in (k_z^{\min}, k_z^{\max})$ dictated by the topology. Hence the string connection between members of a monopole-antimonopole pair with the same k_y (and opposite k_z) is protected by the symmetry and dictated by the topology.

It is noted from Fig. 3(b) that in case (ii) the two Fermi arcs are actually connected together as $k_y^c = -k_y^c$, forming a closed Fermi surface. In the four-Dirac-cone case in Fig. 3(a), when $k_y^c \neq -k_y^c$, the Fermi surface is not closed. It seems that the Fermi arcs are also invariant under the inversion operation $k_y \to -k_y$. However, this is only a special property of zero-energy surface states due to the particle-hole symmetry. For surface states with nonzero energy, the spectral functions are not k_y-inversion symmetric as the boundary breaks the $(x,y) \to (-x,-y)$ inversion symmetry. To illustrate the surface states explicitly, we plot the spectral functions of the surface states in Figs. 4(a) and 4(b) for the two cases that correspond to Figs. 3(a) and 3(b), respectively. The selected energies of the surface states from left to right (in both the $k_y < \pi$ and $k_y > \pi$ regions) are -0.8, -0.4, 0, 0.4, and 0.8, respectively. For each energy there are two arcs: one in the $k_y < \pi$ region and another in the $k_y > \pi$ region. For example, both the leftmost arc in the $k_y < \pi$ region and the leftmost arc in the $k_y > \pi$ region have energy $E = -0.8$. It is clearly seen that the spectra are not invariant under k_y inversion but invariant under the particle-hole transformation. In addition, only the arcs with zero energy link between the monopoles whereas other arcs merge into the bulk bands without going through the Weyl points. Finally, it is seen from Fig. 3(d) that the two Fermi arcs are assigned to two different chiral edge states at the left boundary, which both have positive group velocity along the z direction. It is found that the shape of the Fermi arcs can be tuned via ϕ_1 and ϕ_2 to be curved in [as in Fig. 3(b)], curved out, or flat [as in Fig. 3(a)]. Flat bands can be interesting in the context of elevated transition temperatures in spontaneous symmetry breaking [7], as the density of states is increased.

VI. A POSSIBLE SCHEME FOR EXPERIMENTAL REALIZATION

In this section we propose a possible scheme to realize the model in optical lattices. The required artificial gauge fields are generated by spatial variation of the laser-atom interaction as suggested in Ref. [27]. Suppose that there is an excited state with energy much higher than the energy scale where the above model is defined. Impose standing waves of light to induce the following coupling between the ground and excited states in the rotating-wave approximation:

$$H_R(\mathbf{r}) = M[\cos 2\pi z \cos \pi(x+y)\hat{F}_x + \cos \pi(x-y)\hat{F}_y + \zeta \hat{F}_z], \tag{12}$$

where $\hat{F}_\nu$ ($\nu = x,y,z$) are the Pauli matrices acting on the (dressed) ground and excited states. M and ζ are parameters of the laser-atom coupling. This scheme can be realized in a system with three standing-wave Raman lasers with a detuning of $M\zeta$ [27]. The three laser wave vectors are $(\pi,\pi,\pm 2\pi)$ and $(\pi,-\pi,0)$, and the kinetic energy is small compared to the energy splitting of the local dressed states [i.e., the eigenstates of the local Hamiltonian $H_R(\mathbf{r})$]. The emergent gauge fields can be obtained via the Berry phase [27], $\mathbf{A} = \langle \Psi_G(\mathbf{r}) | i\nabla_{\mathbf{r}} | \Psi_G(\mathbf{r}) \rangle$ with $|\Psi_G(\mathbf{r})\rangle$ being the ground state of the local Hamiltonian $H_R(\mathbf{r})$. One can show that $\mathbf{A} = \frac{1}{2}\Theta\nabla_{\mathbf{r}}\Pi$ where $\Theta = 1 - \frac{|\zeta|}{\sqrt{\cos^2(2\pi z)\cos^2\pi(x+y)+\cos^2\pi(x-y)+\zeta^2}}$ and $\Pi = \mathrm{Arg}[\cos(2\pi z)\cos\pi(x+y) + i\cos\pi(x-y)]$. The effective "magnetic field" (i.e., the Berry curvature, or the "magnetic flux density") is written as $B_\nu = \varepsilon^{\nu\delta\rho}\partial_\delta A_\rho$, with $\nu,\delta,\rho = x,y,z$ and ε the Levi-Cività tensor. The plaquette flux for each plaquette is the "magnetic flux" through it. For example, for a plaquette in the x-y plane, the plaquette flux is $\Phi = \int dx\, dy\, B_z$, where the integral is limited within the plaquette. We plot the effective magnetic field B_z through the x-y plane (in odd layers) and $B_{[1\bar{1}0]}$ through the $(1\bar{1}0)$ plane in Figs. 5(a) and 5(b), respectively. It is seen that the magnetic flux density has exactly the same checkerboard pattern as the plaquette

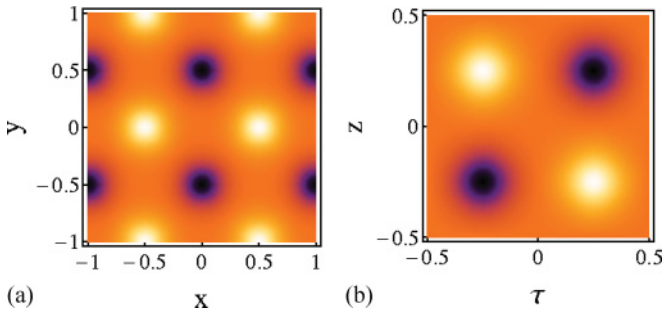

FIG. 5. (Color online) The magnetic flux density through (a) the (001) plane at an odd layer; (b) the $(1\bar{1}0)$ plane. $\tau = \mathbf{r}\cdot(1,1,0)/2 = (x+y)/2$. The bright region has positive and the dark region negative value.

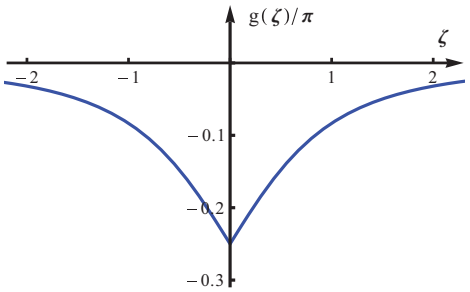

FIG. 6. (Color online) The function $g(\zeta)$.

fluxes in Figs. 1(a) and 1(b). This shows that the gauge field generated by the Hamiltonian, Eq. (12) is exactly what is needed for the realization of the model. The magnetic flux density in the (110) plane is zero everywhere, because the current scheme realizes the model with $\phi_1 = \phi_2$.

The phase along a hopping path l is given by $\phi_l = \int_l d\mathbf{r} \cdot \mathbf{A}$. Combining this with Figs. 1(a) and 1(b), one can show that the hopping phases ϕ_1 and ϕ_2 in the Hamiltonian Eq. (4) are given by

$$\phi_1 = \phi_2 = g(\zeta), \tag{13}$$

whereas the phases of other hoppings are zero. The function $g(\zeta)$ is plotted in Fig. 6. $\phi_1 = \phi_2 \in [-\pi/4,0]$. Due to the factor $\cos(2\pi z)$ the gauge phases are inverted from the odd layers at $z = n$ to the even layers at $z = n + \frac{1}{2}$ with n being integer. This exactly realizes the lattice structure in Fig. 1. The amplitudes and signs of the remaining hoppings can, in principle, be tuned via various optical lattice techniques [32]. By manipulation of the ratio $t_2/t_\perp$, the system can experience various phases in the phase diagram: (i) At finite ϕ_1 when $|t_2/t_\perp| < 1$ it is a Weyl semimetal; (ii) otherwise it is a QAH insulator with $C_{xy}(k_z) = 2\mathrm{sgn}[t_1 t_2 t_\perp \sin(2\phi_1)]$ for all k_z. (iii) At $\phi_1 = 0$ the system is always a nontopological semimetal.

VII. SUMMARY

In summary, a model of a simple-cubic lattice with staggered fluxes which exhibits a Weyl semimetal phase is proposed and studied. The model is simple and can act as a prototype to study the properties of Weyl semimetals. Due to its simplicity, the model is potentially achievable both in ultracold fermions in optical lattices and in condensed-matter systems. In particular, we propose a possible scheme to realize the model in an optical lattice system. Unlike previous works, here the mechanism to achieve the topological Weyl semimetal state is to gap the quadratic-band touching by time-reversal-symmetry-breaking hoppings. The system exhibits a rich phase diagram, where the number of Weyl fermions and their topological charges and positions are tunable via the plaquette fluxes (hopping phases). The Weyl semimetal state is demonstrated to be the intermediate phase between a nontopological semimetal and a quantum anomalous Hall insulator. The transitions between those phases can be understood via the evolution of the Weyl points (see below). As the Weyl points move and split (or merge) via the manipulation of the hopping phases, the Fermi arcs and surface states undergo significant change, as the Fermi arcs have to be terminated at the Weyl points.

The relations between nontopological insulators or semimetals, topological Weyl semimetals, and QAH insulators demonstrated in this paper can be summarized in the following processes: (i) A nontopological insulator becomes a nontopological semimetal via forming an accidental band-touching node with winding number $N_w = 0$. (ii) By splitting the node into pairs of Weyl fermions with opposite topological charges and moving the positively and negatively charged Weyl fermions in opposite directions in $\mathbf{k}$ space, a Weyl semimetal state is created. (iii) When the positively and negatively charged Weyl points are moved by half of the reciprocal lattice vector, they merge and annihilate each other in pairs, making the system transit into a QAH insulator. The sign of the Chern number of the QAH state depends on the direction along which the Weyl fermions are moved. Quantized Berry fluxes are inserted into the bulk states during the evolution because Weyl fermions are the monopoles of Berry-phase gauge fields. This picture can be generalized to understand the relations between the nontopological insulators or semimetals, the time-reversal-symmetric topological Weyl semimetals, and the 3D quantum spin Hall insulator (i.e., the time-reversal-invariant Z_2 topological insulators), where quantized non-Abelian Berry fluxes are inserted into the bulk states during the moving of the monopoles.

ACKNOWLEDGMENTS

Work at the Weizmann Institute was supported by the German Federal Ministry of Education and Research (BMBF) within the framework of the German-Israeli cooperation project (DIP) and by the Israel Science Foundation (ISF). I thank Zhong Fang, Xi Dai, Jonathan Ruhman, and Zohar Ringel for illuminating discussions and comments.

[1] S. Adler, Phys. Rev. **177**, 2426 (1969); J. S. Bell and R. Jackiw, Nuovo Cimento A **60**, 47 (1969).

[2] A. K. Geim and K. S. Novoselov, Nat. Mater. **6**, 183 (2007).

[3] A. H. Castro Neto, F. Guinea, N. M. R. Peres, K. S. Novoselov, and A. K. Geim, Rev. Mod. Phys. **81**, 109 (2009); N. M. R. Peres, *ibid.* **82**, 2673 (2010).

[4] S.-L. Zhu, B. Wang, and L.-M. Duan, Phys. Rev. Lett. **98**, 260402 (2007); B. Wunsch, F. Guinea, and F. Sols, New J. Phys. **10**, 103027 (2008); C. Wu and S. Das Sarma, Phys. Rev. B **77**, 235107 (2008); G. Montambaux, F. Piéchon, J.-N. Fuchs, and M. O. Goerbig, *ibid.* **80**, 153412 (2009); K. L. Lee, B. Grémaud, R. Han, B.-G. Englert, and C. Miniatura, Phys. Rev. A **80**, 043411 (2009); N. Goldman, A. Kubasiak, A. Bermudez, P. Gaspard, M. Lewenstein, and M. A. Martin-Delgado, Phys. Rev. Lett. **103**, 035301 (2009).

[5] Note that, in this paper, we focus on a system with two bands touching (pseudo-spin-1/2 system). Massless Dirac fermions with higher pseudospins have also been studied in ultracold

fermions in optical lattices recently [see, e.g., D. Bercioux, D. F. Urban, H. Grabert, and W. Häusler, Phys. Rev. A **80**, 063603 (2009); Z. Lan, N. Goldman, A. Bermudez, W. Lu, and P. Öhberg, Phys. Rev. B **84**, 165115 (2011); B. Dóra, J. Kailasvuori, and R. Moessner, *ibid.* **84**, 195422 (2011)]; some intriguing properties were demonstrated, such as multirefringence Klein tunneling and flat bands. It is found that the half-integer-spin system can be described as a collection of spin-1/2 systems. Hence the picture and results presented in this paper can be extended to the higher-spin situation with half-integer spin.

[6] Recent studies [23,24] also indicate that topological pairing states with *odd* Chern numbers are favored at zero (low) temperature and finite chemical potential in the weak-pairing regime when chiral fermions undergo the pairing interaction within each flavor.

[7] G. E. Volovik, *The Universe in a Helium Droplet* (Clarendon, Oxford, 2003); in *Quantum Analogues: From Phase Transitions to Black Holes and Cosmology*, edited by W. Unruh and R. Schützhold, Lecture Notes in Physics, Vol. 718 (Springer, Berlin, 2007), p. 31; e-print arXiv:1111.4627.

[8] H. Nielssen and N. Ninomiya, Phys. Lett. B **130**, 389 (1983).

[9] There are some early studies that are summarized in Ref. [7]. Also in Ref. [8] it was proposed that some gapless semiconductors with broken inversion symmetry can be candidates for Weyl semimetals.

[10] S. Murakami, New. J. Phys. **9**, 356 (2007).

[11] L. Balents, Physics **4**, 36 (2011).

[12] X. Wan, A. M. Turner, A. Vishwanath, and S. Y. Savrasov, Phys. Rev. B **83**, 205101 (2011).

[13] A. A. Burkov and L. Balents, Phys. Rev. Lett. **107**, 127205 (2011).

[14] A. A. Burkov, M. D. Hook, and L. Balents, Phys. Rev. B **84**, 235126 (2011).

[15] G. B. Halász and L. Balents, Phys. Rev. B **85**, 035103 (2012).

[16] G. Xu, H. Weng, Z. Wang, X. Dai, and Z. Fang, Phys. Rev. Lett. **107**, 186806 (2011).

[17] C. Fang, M. J. Gilbert, X. Dai, and B. A. Bernevig, e-print arXiv:1111.7309.

[18] G. Y. Cho, e-print arXiv:1110.1939; H. Jiang, Z. Qiao, H. Liu, and Q. Niu, Phys. Rev. B **85**, 045445 (2012).

[19] J. L. Mañes, e-print arXiv:1109.2581; S. M. Young *et al.*, e-print arXiv:1111.6483 [Phys. Rev. Lett. (to be published)].

[20] P. Hosur, S. Ryu, and A. Vishwanath, Phys. Rev. B **81**, 045120 (2010); A. Bermudez, L. Mazza, M. Rizzi, N. Goldman, M. Lewenstein, and M. A. Martin-Delgado, Phys. Rev. Lett. **105**, 190404 (2010).

[21] K. Sun, W. V. Liu, A. Hemmerich, and S. Das Sarma, Nat. Phys. **8**, 67 (2012).

[22] K. Sun, H. Yao, E. Fradkin, and S. A. Kivelson, Phys. Rev. Lett. **103**, 046811 (2009).

[23] J.-H. Jiang and S. Wu, e-print arXiv:1107.4274.

[24] J.-H. Jiang, e-print arXiv:1110.2043.

[25] Y. Lin *et al.*, Nature (London) **462**, 628 (2009); J. Dalibard *et al.*, Rev. Mod. Phys. **83**, 1523 (2011).

[26] D. Jaksch and P. Zoller, New J. Phys. **5**, 56 (2003); E. J. Mueller, Phys. Rev. A **70**, 041603 (2004); F. Gerbier and J. Dalibard, New J. Phys. **12**, 033007 (2010); M. Aidelsburger, M. Atala, S. Nascimbene, S. Trotzky, Y. A. Chen, and I. Bloch, Phys. Rev. Lett. **107**, 255301 (2011).

[27] N. R. Cooper, Phys. Rev. Lett. **106**, 175301 (2011); B. Béri and N. R. Cooper, *ibid.* **107**, 145301 (2011).

[28] L. Mazza *et al.*, New J. Phys. **14**, 015007 (2012).

[29] For example, T. Rueckes *et al.*, Science **289**, 94 (2000); I. Kuzmenko, S. Gredeskul, K. Kikoin, and Y. Avishai, Phys. Rev. B **67**, 115331 (2003); Y. Iye, E. Kuramochi, M. Hara, A. Endo, and S. Katsumoto, *ibid.* **70**, 144524 (2004).

[30] N. Nagaosa and Y. Tokura, Phys. Scr. **2012**, 014020 (2012).

[31] X. Dai, T. L. Hughes, X.-L. Qi, Z. Fang, and S.-C. Zhang, Phys. Rev. B **77**, 125319 (2008).

[32] The sign of hopping can be tuned by some subtle techniques. For example, in laser-assisted tunnel hopping [26], the hopping phase can be tuned by the laser. If the phase is $\pm\pi$, then the sign of the hopping will be changed.